Image warping waveform tomography

Francesco Perrone and Paul Sava, Center for Wave Phenomena, Colorado School of Mines*

SUMMARY

Imaging changes of physical parameters in the subsurface requires an estimate of the long wavelength component of the same parameters in order to reconstruct the kinematics of the waves propagating in the subsurface. The model is unknown and must be estimated from the same data. One can try to reconstruct the model by matching the recorded data with simulated waveforms extrapolated in a trial model. Alternatively, also assuming a trial model, one can obtain a set of images of the reflectors from a number of seismic experiments and match the locations of the imaged interfaces. Apparent displacements between migrated images contain information about the velocity model and can be used for velocity analysis. We derive an image-domain wavefield tomography procedure using the displacement vectors obtained by image warping. Our objective function is related to the known image difference objective function by a Taylor series expansion of the warped images with respect to the warping vectors. Image warping allows us to effectively perform phase unwrapping in the image domain, thus making shot-based migration velocity analysis more robust against cycle skipping.

INTRODUCTION

Accurate propagation velocities in the subsurface are crucial in seismic imaging and exploration geophysics. A kinematically accurate velocity model allows us to correctly reconstruct Green functions and thus precisely image the subsurface discontinuities responsible for the data acquired at the surface or in boreholes. An accurate image of the geologic structure is key for planning drilling operations and for reducing hazards associated with drilling through faults. Seismic propagation velocities are sensitive to the stress conditions in the subsurface and carry information about the orientation of the principal stresses and overpressure (Carcione, 2007), which are both important for mitigating hazards during drilling operations and reducing risk in production.

A main distinction has been drawn between methods that recover the velocity model by matching the recorded data with simulated synthetic wavefields modeled in a trial velocity model (Tarantola, 1984; Pratt, 1999), and methods that focus on optimizing the migrated images (Fowler, 1985; Faye and Jeannot, 1986; Al-Yahya, 1989; Biondi and Sava, 1999; Albertin et al., 2006). Full-waveform inversion (FWI) is the name used to indicate techniques that operate in the data domain and minimize some functional of the data residual. Migration velocity analysis (MVA) identifies all methods that reconstruct the velocity model by analyzing the similarity between migrated images. FWI is simple to implement, but it is very sensitive to every inconsistency between the recorded and modeled data. It requires an accurate parametrization of the physics of wave propagation, knowledge of the source signature, and a kinematically reliable starting model in order to converge to the global minimum of the objective function (Santosa and Symes, 1989; Kelly et al., 2010). MVA is not as sensitive to errors in the source signature and it is more robust against errors in the initial velocity model; it is characterized by an objective function which is convex over a wide range of model perturbations and thus more suitable for gradient-based optimization procedures. Nonetheless, as it ignores the amplitude information in the data for inversion purposes, MVA cannot achieve the high-resolution results that FWI promises in the ideal scenario. MVA is conventionally used to produce a kinematically accurate model to initialize FWI for refining the velocity with high-resolution details.

This paper deals with the estimation of the velocity model using image warping. Perrone et al. (2012) show how the apparent displacement field estimated between two images can be used to measure velocity errors with a minimum number of migrated images, and they design a linearized wave-equation migration velocity analysis (WEMVA) algorithm based on the method developed by Sava and Biondi (2004). The WEMVA operator in Perrone et al. (2012) is obtained from the phase-shift continuation operator and several linearizations with respect to the wavefield and wavenumber (Born approximation). The entire inversion procedure stems from the particular form of the extrapolation operator that allows one to derive a linearized operator which links perturbation in the image space to perturbation in the model (slowness) parameters. Because of the strong assumption of a phase-shift continuation wave-extrapolator, this method cannot be applied to images obtained using different engines (for example, with reverse-time migration). Here, we extend the linearized wave-equation migration velocity analysis algorithm of Perrone et al. (2012) to incorporate a two-way extrapolation engine and to directly exploit the displacement field. The displacement vector field is used to estimate an image perturbation, then through single scattering Born modeling, the wavefield perturbation due to the image perturbation is computed. The correlation between the scattered and background wavefields represents the kernel for the model update.

THEORY

Perrone et al. (2012) introduce a measure of velocity error for migration velocity analysis exploiting the con-

sistency between the orientation of structural features in the image and the apparent displacement between two migrated images. The error measure $\mathcal{J}$ is the energy of the projection of the displacement vector $\mathbf{u}(\mathbf{x})$ onto the dip vector $\boldsymbol{\nu}(\mathbf{x})$

$$\mathcal{J}(m) = \frac{1}{2}\left\|\nabla R \cdot \mathbf{u}\right\|^2, \tag{1}$$

where $m(\mathbf{x})$ represents the model parameter (slowness, slowness squared, or velocity) as a function of position $\mathbf{x}$. The image gradient ∇R is parallel to the dip vector $\boldsymbol{\nu}(\mathbf{x})$, which is defined as the vector normal to the structure at position $\mathbf{x}$, but changes sign across the reflector; and the displacement vector $\mathbf{u}(\mathbf{x})$ is also a function of the position vector $\mathbf{x}$. Displacement vectors $\mathbf{u}$ are obtained by an iterative search for the maximum of local correlations and warping of the input images; this method, first applied to measuring the apparent shift between migrated images in 4D seismic processing, is described in detail by Hale (2007). The image gradient is a linear functional of the migrated image, and we can use perturbation theory to compute the variation with respect to the model parameters.

The displacement vector field is obtained by picking the correlation lag that maximizes the local correlation panels:

$$\mathbf{u}(\mathbf{x}) = \arg\max_{\boldsymbol{\lambda}} c(\mathbf{x}, \boldsymbol{\lambda}), \tag{2}$$

where $c(\mathbf{x}, \boldsymbol{\lambda}) = \int_{w(\mathbf{x})} R_i\left(\boldsymbol{\xi} - \frac{\boldsymbol{\lambda}}{2}\right) R_{i+1}\left(\boldsymbol{\xi} + \frac{\boldsymbol{\lambda}}{2}\right) d\boldsymbol{\xi}$ is the local correlation of two images $R_i(\mathbf{x})$ and $R_{i+1}(\mathbf{x})$, and $w(\mathbf{x})$ is are seamless overlapping windows. The arg max operator is not differentiable and thus we cannot compute the Frechét derivative with respect to the model parameters directly.

The dot product between the gradient of the migrated image and the apparent displacement field between two images (equation 1) is a linear approximation of the image difference with respect to the displacement vector (Perrone et al., 2012). Compared to the image difference, equation 1 is less affected by amplitude differences due to the change of the shot location and is less prone to cycle skipping problems because warping maps every event in one image to the corresponding event in the second image. The relation between image difference and the dot product of image gradient and displacement field can be used to set up a wavefield tomography procedure based on the image difference objective function, but more robust.

We interpret the residual $\nabla R \cdot \mathbf{u}$ as the mismatch between the updates of the small wavelengths of the model parameters obtained from adjacent shots. This approach is related to the work of Xu et al. (2012), who follow a two-step, migration/demigration procedure to better condition FWI for reflection data. Another work on a similar path is the differential waveform inversion presented by Chauris and Plessix (2012) in the framework of FWI. Here, we set up the problem in the image domain, i.e. in the framework of migration velocity analysis. The demigration approach reduces the computational cost and complexity with respect to the adjoint-state calculations and greatly simplifies the implementation and the physical interpretation of the method. Of course, since we are approximating the image difference with our image warping procedure and we are not constructing the exact gradient for the objective function in equation 1, we are introducing a systematic error in the procedure. Quantifying the error requires the exact computation of the gradient of the objective function in equation 1; the displacement vectors are obtained from a non differentiable procedure (see equation 2) but they can be linked to the model parameters using a multidimensional generalization of the connective function method developed by (Luo and Schuster, 1991). However, this multidimensional extension is considerably more computationally expensive than the method proposed in this work.

The adjoint-state calculations for the image difference objective function are well-known in the literature (Plessix, 2006). The adjoint sources $g_{s_i}(\mathbf{x}, t)$ and $g_{r_i}(\mathbf{x}, t)$ for the image-difference objective function depend on the second derivative of the migrated images along the shot axis of the prestack image cube and the wavefields computed in the background model (Plessix, 2006):

$$g_{s_i} = (R_{i-1} - 2R_i + R_{i+1})\, u_{ri} \tag{3}$$

$$g_{r_i} = (R_{i-1} - 2R_i + R_{i+1})\, u_{si}. \tag{4}$$

The functions in equation 3 are the force terms for the wavefield extrapolations

$$\mathcal{L}(m)\, a_{si} = g_{s_i} \;\; \mathcal{L}(m)\, a_{ri} = g_{r_i}, \tag{5}$$

where $a_{s_i}(\mathbf{x}, t)$ and $a_{r_i}(\mathbf{x}, t)$ are the adjoint wavefields. The adjoint sources generate the scattered fields due to the reflectivity perturbation $(R_{i-1} - 2R_i + R_{i+1})$. These wavefields can also be interpreted as the *demigrated* reflectivity perturbation. The gradient of the objective function is then the zero-lag time correlation of the background and adjoint wavefields (Fichtner et al., 2006; Plessix, 2006). We see that uneven illumination of the subsurface may lead to spurious adjoint sources and gradients of the objective function. Even more important than illumination, cycle skipping may arise when the velocity model is severely inaccurate, because different images map the same structures at inconsistent positions in the subsurface.

We replace $(R_{i-1} - 2R_i + R_{i+1})$ with an approximation derived from image warping. The apparent displacement field performs phase unwrapping in the image domain and removes the cycle skipping problem by warping one image into its neighbor. Let us indicate with $\mathbf{u}_{i-1}$ and $\mathbf{u}_i$ the apparent displacement field that warps R_{i-1} into R_i and R_i into R_{i+1}, respectively. We can construct approximations of the image differences by computing the dot product of the image gradient with the displacement fields. In order to guarantee symmetry with respect to the ith shot, we use R_i to construct the

image perturbations

$$\Delta R_{i-1} = R_i - R_{i-1} \approx \nabla R_i \mathbf{u}_{i-1} \quad (6)$$

$$\Delta R_i = R_{i+1} - R_i \approx \nabla R_i \mathbf{u}_i. \quad (7)$$

Using the expressions in equations 6-7, we approximate the second derivative along the shot axis with

$$R_{i-1} - 2R_i + R_{i+1} \approx \Delta R_i - \Delta R_{i-1}, \quad (8)$$

which is robust against cycle skipping, and it is less sensitive to uneven illumination because the amplitude effects are absorbed in the displacement fields.

NUMERICAL EXAMPLES

We test image warping wavefield tomography using a model with a horizontal reflector at 2 km depth in a homogeneous background and compare our methodology with the direct image difference tomography approach proposed by Plessix (2006) to regularize full-waveform inversion. Image warping effectively performs phase unwrapping in the image domain and produces higher quality gradients with respect to the image difference approach.

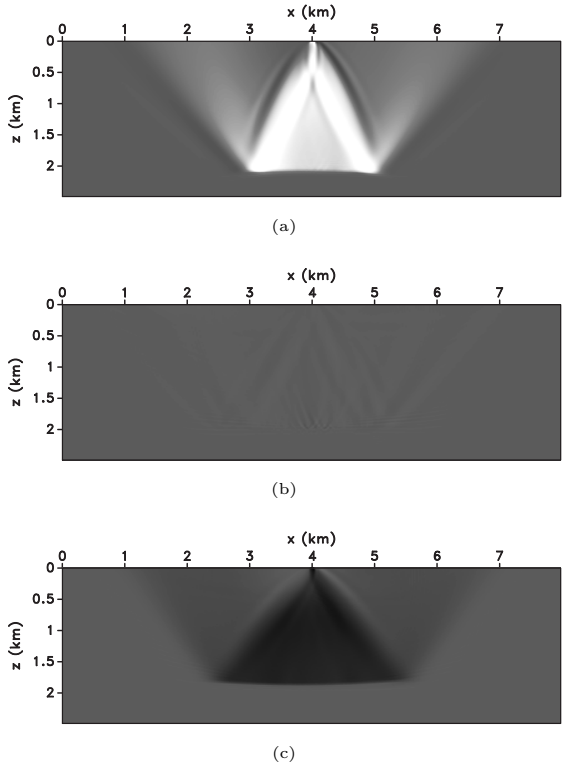

Figure 1: Sensitivity kernels obtained using *image warping* wavefield tomography for (a) high, (b) correct, and (c) low velocities.

In order to measure errors in the velocity model, we analyze two nearby shots: the position of the first shot is

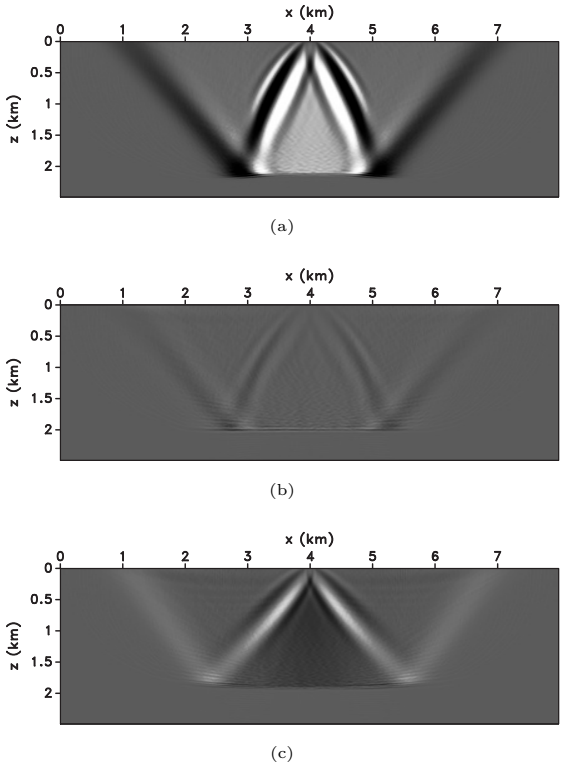

Figure 2: Sensitivity kernels obtained using *image difference* wavefield tomography for (a) high, (b) correct, and (c) low velocities.

$x = 3.8$ km and the distance between the shots is 200 m. We apply different homogeneous perturbations to the velocity model, then migrate the data, and finally construct the sensitivity kernels in Figure 1. These sensitivity kernels are obtained by correlating the background wavefields (used for migration) with the scattered wavefields excited by the interaction of the background wavefields with the reflectivity perturbation computed from equation 8. The gradient is smooth over the entire extent of the reflector when the velocity is incorrect and has negligible value when the model is correct.

By comparison, Figures 2 shows the gradients obtained for the same perturbations using the image-difference objective function. Notice the strong side lobes at the edges of the reflector, where we observe cycle skipping because the overlap between the images is not enough. The gradients are noisier than the ones obtained using image-warping.

We also test our approach on the Marmousi model. We model 100 shots separated by 80 m. The spatial sampling is 8 m in both x and z directions. Receivers are located at every grid point on the surface. The data are modeled without free-surface multiples, but internal multiples are present in the data. We assume that free-surface multiples can be effectively removed from the data using a technique like SRME (Verschuur, 1991).

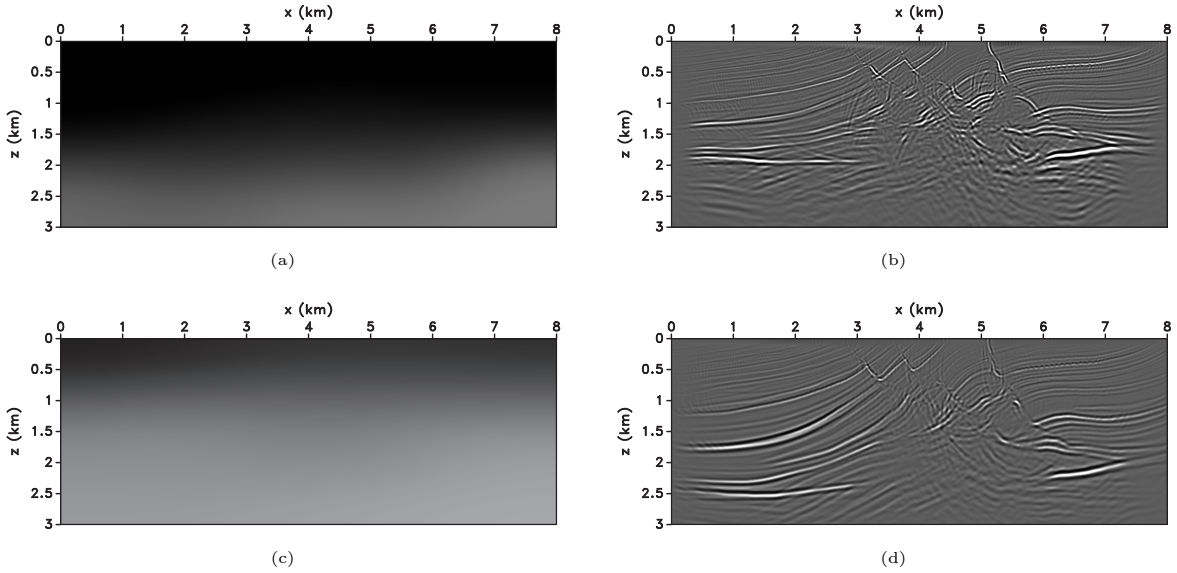

Figure 3: (a) The initial model represented by an incorrect $v(z)$ velocity. (b) The migrated image is distorted and not interpretable in the central part of the model. Observe the general upward shift of the image due to the bias in the velocity model. (c) Velocity model after 50 iteration of wavefield tomography and (d) corresponding migrated image. The reflectors shift toward their correct location, and the truncation of the beds against the fault walls improves.

The initial model is obtained by filtering the exact Marmousi model with a triangular smoother with radius 120 samples vertically and 200 samples horizontally. The smooth model is then biased with a -0.4 km/s homogenous perturbation (Figure 3(a)). The migrated image obtained using this model is shown in Figure 3(b). The central part of the image is non interpretable and all reflectors are mispositioned and defocused; the deep and strong reflectors are shifted about 500 m upward because of the bias toward low velocities in the initial velocity model. The noise in the image is due to the strong errors in the migration model and the inconsistent imaging of the reflectors from different shots. Also, the internal multiples in the data are not imaged correctly since migration is based on single scattering assumptions.

We run inversion to recover the general trend of the velocity model using image warping wavefield tomography. Illumination compensation and regularization is crucial to update the edges of the model and to balance the strength of the update between the sides of the model, which are characterized by simple sedimentary structures, and the central part of the model, where the faults and discontinuities of the reflectors complicate the wavefields. The model update is structurally-oriented smoothed using the orientation of the reflectors in the complete image. The length of the smoothing filter is 100 samples along and 50 samples across the structure. The inversion reaches a floor after about 50 iterations and returns the velocity model in Figure 3(c) and the associated migrated image in Figure 3(d). In the final image, the reflectors are shifted toward their correct location. We improve the truncation of the sedimentary beds against the fault walls around $z = 1$ km and $x = 3.5$ km. The migration frowns, visible at $x = 3$ km in the original image and due to the discontinuities of the sediments at the fault locations, are corrected by the inversion procedure and disappear in the final image. The reservoir (at about $x = 2.5$ km and $z = 5.5$ km) is still poorly imaged, but we are able to recover the long wavelength trend of the velocity model. Further inversion iterations with milder regularization are needed to recover higher resolution details of the model and accurately image the reservoir area. The image-difference objective function for wavefield tomography in the migrated-shot domain can be made more robust using image warping. Displacement fields warping a migrated image into the image obtained from a neighboring experiment absorb amplitude differences due to the shift in source location and remove cycle skipping, because every reflector in one image is mapped into the corresponding event in the other image. The objective function based on the warping relation between the images is able to measure the distance between different models, and to highlight the most coherent images, thus enabling local gradient-based optimization.

ACKNOWLEDGMENTS

This work was supported by the sponsors of the Consortium Project on Seismic Inverse Methods for Complex Structures. The reproducible numerical examples in this paper use the Madagascar open-source software package freely available from http://www.ahay.org and the Mines JTK freely available at https://github.com/dhale/jtk.

REFERENCES

Al-Yahya, K., 1989, Velocity analysis by iterative profile migration: Geophysics, **54**, P. 718–729.

Albertin, U., P. Sava, J. Etgen, and M. Maharramov, 2006, Adjoint wave-equation velocity analysis: Presented at the 74th Ann. Internat. Mtg., SEG.

Biondi, B., and P. Sava, 1999, Wave-equation migration velocity analysis: Presented at the 69th Ann. Internat. Mtg., SEG.

Carcione, J., 2007, Wave fields in real media wave propagation in anisotropic, anelastic, porous and electromagnetic media: Elsevier. Handbook of Geophysical Exploration.

Chauris, H., and R.-E. Plessix, 2012, Investigating the differential waveform inversion: Presented at the 74th EAGE Conference & Exhibition - Workshops, EAGE.

Faye, J.-P., and J.-P. Jeannot, 1986, Prestack migration velocity analysis from focusing depth imaging: Presented at the 56th Ann. Internat. Mtg., Soc. of Expl. Geophys.

Fichtner, A., H.-P. Bunge, and H.Igel, 2006, The adjoint method in seismology I. theory: Physics of the Earth and Planetary Interiors, 86–104.

Fowler, P., 1985, Migration velocity analysis by optimization: Technical Report 44, Stanford Exploration Project.

Hale, D., 2007, A method for estimating apparent displacement vectors from time-lapse seismic data: Technical Report CWP-566, Center for Wave Phenomena, Colorado School of Mines.

Kelly, S., J. R. Martinez, B. Tsimelzon, and S. Crawley, 2010, A comparison of inversion results for two full-waveform methods that utilize the lowest frequencies in dual-sensor recordings: Presented at the 80th Ann. Internat. Mtg., Soc. of Expl. Geophys.

Luo, Y., and G. T. Schuster, 1991, Wave-equation traveltime inversion: Geophysics, **56**, 645–653.

Perrone, F., P. Sava, C. Andreoletti, and N. Bienati, 2012, Linearized wave-equation migration velocity analysis by image warping: Submitted to Geophysics.

Plessix, R.-E., 2006, A review of the adjoint-state method for computing the gradient of a functional with geophysical applications: Geophys. J. Int., **167**, 495–503.

Pratt, R. G., 1999, Seismic waveform inversion in the frequency domain, part 1: Theory and verification in a physical scale model: Geophysics, **64**, 888–901.

Santosa, F., and W. W. Symes, 1989, An analysis of least-squares velocity inversion, *in* Geophysical Monograph no. 4: Soc. of Expl. Geophys.

Sava, P., and B. Biondi, 2004, Wave-equation migration velocity analysis. I. Theory: Geophysical Prospecting, **52**, 593–606.

Tarantola, A., 1984, Inversion of seismic reflection data in the acoustic approximation: Geophysics, **49**, 71–92.

Verschuur, D. J., 1991, Surface-related multiple elimination, an inversion approach: PhD thesis, Technische Univ., Delft (Netherlands).

Xu, S., D. Wang, F. Chen, and Y. Zhang, 2012, Full waveform inversion for reflected seismic data: Presented at the 74th Conference and Exhibition, EAGE.